Accepted for publication in Composite Structures

Published in February 13, 2014

DOI: 10.1016/j.compstruct.2014.02.003

Finite element method assisted stiffness design procedure for non-circular profile composite wastewater pipe linings

Gergely Czél[a], T. Czigány[a,b]

[a]Department of Polymer Engineering, Faculty of Mechanical Engineering, Budapest University of Technology and Economics
Műegyetem rkp. 3., H-1111 Budapest, Hungary
[b]MTA-BME Research Group for Composite Science and Technology,
Műegyetem rkp. 3., H-1111 Budapest, Hungary.
Corresponding author: Gergely Czél
E-mail: czel@pt.bme.hu
Telephone: 003614631462

Abstract

The elastic behaviour of filament wound egg shape profile glass/polyester composite wastewater pipe linings was analysed with the scope of developing a simple stiffness sizing method. Ring compression tests were executed and simulated with the finite element (FE) method to verify the modelling concept. Good agreement has been confirmed, and a more realistic pipe-in-pipe type model was developed to simulate the operational loads and deformations of the liner pipes. Using the FE model outputs a 10 parameter function of the three most important material and geometric parameters was fitted to describe the defined stiffness of specific pipe cross sections. A unique design chart was developed representing the deformations of given cross section liner pipes of a wide range of stiffness values in function of the applied outer pressure.

Keywords: Composite pipe, oval profile, pipe-in-pipe, no-dig, trenchless rehabilitation

1. Introduction

Composites made of thermosetting polymer matrix and glass fibre reinforcing materials show high tensile strength, relatively low elastic modulus, low density and high chemical resistance compared to steel. These beneficial properties have made polymer composites attractive for the piping industry, where low maintenance need of these materials is also highly appreciated [1].

Besides traditional applications such as pressure piping and large vessels, polymer composites are successfully applied for underground pipe lining with special trenchless (no-dig) technologies [2]. This is of very high interest since the main collector sewers under several cities around the world including London, Paris, Hamburg, New York, Los Angeles, Newark [3], Kolkata [4]-[6], Mumbai and Delhi were constructed around the end of the 19th century, more than 100 years ago using various non-circular, usually oval, egg or horseshoe shape profiles. Although a lot of the original sewers are still fully functional due to regular maintenance, they exceeded their design lifetime decades ago. Therefore hundreds of kilometres of the non-circular profile underground sewer pipe network needs urgent rehabilitation due to leakage, sedimentation and structural deterioration.

Polymer composite pipes are especially useful for trenchless pipe lining purposes which can cut down disruption to surface traffic significantly during rehabilitation of underground pipes. Various forming technologies of composites such as injecting, and prepreg technologies make them capable of being flexible during insertion into the old pipe, and they can be cured in situ. Wide spectrum of trenchless lining technologies is available for water, gas and sewerage piping, including ones for non-circular profile pipes. One of the most common lining technologies for non-circular (typically egg or oval shaped) man-accessible sewer pipes is the “short pipe” or slip-lining process [7], where prefabricated (cured) liner pipe sections usually made of fibreglass reinforced thermosetting resins are pulled or pushed into the old pipe [3]-[6],[8]. This type of lining technology is applied in those cases, where the load bearing capacity of the old pipe is acceptable, but it is leaking due to longitudinal or other types of cracks in the rigid, usually concrete or brick pipe walls. The main load of the

lining in this case is the outer hydrostatic pressure coming from the groundwater, because water can pass through the leaks and possible grouting between the old and new pipe. Researchers such as Boot and Welch [9],[10], Zhao [11] and Thépot [12],[13] normally take the outer pressure into consideration as the only load on the lining. Analytical buckling theories published first by Timoshenko [14] and modified by numerous researchers are valid for circular profiles, and utilizes the geometric and elastic constants of the pipe. In case of a non-circular lining, analytical models are too complicated and the finite element (FE) method offers accurate solutions [10],[15],[16], rather for elastic problems than for failure and damage analysis. Ikram and Abdennour [17] modelled various non-circular profiles under concentrated compressive loads and established shape factors for them. This method helps relating the elastic behaviour of irregular profiles to that of circular ones. Due to high cost only a few full scale experimental work on the buckling behaviour of flexible non-circular pipe linings has been published. Falter et al [18] tested small and full scale polyethylene egg-shape profile liners subject to outer pressure within their comprehensive study and confirmed that German design code ATV-M 127-2 [19] is adequate for verification purposes.

It is clear from the literature survey that there is a significant demand for a simple stiffness sizing method for non-circular profile wastewater pipe linings subject to outer pressure which can take the manufacturing parameters of filament wound glass fibre reinforced composite pipes such as fibre volume fraction, winding angle and wall thickness into account. This type of quick tool could be utilised along with design codes [19],[20] which usually assume given material properties and could make the design more accurate, saving material, weight and finally cutting down costs and environmental footprint of production, transportation and installation.

The aim of this study is to present a design procedure for stiffness sizing of egg shape profile sewer pipe linings subject to outer pressure loading. A finite element model was constructed to simulate the pipe-in pipe system of the rigid old pipe and the liner, and the results of the simulations were applied for the development of the stiffness sizing procedure. It is of high importance, that once the sizing method is established for a given geometry (cross-section) the finite element software is not necessary for further steps of the calculations. It is very beneficial for small companies with limited budget, that they can mandate a consultant to execute the FEM calculations for a given case (geometry and materials), and then they can use the method without subscribing for the expensive software package.

2. Materials and methods

The developed FE model was validated by comparing the results of ring compression tests to the ones obtained from the numerical model. The tests were executed on egg shape profile ring specimens (see Figure 1.) cut form a filament wound glass fiber reinforced unsaturated polyester composite pipe. The applied ring compression test method is a very basic experimental setup (see Figure 2.), which does not modify the reinforcing structure of the pipe section and for which no special equipment is needed. The ring compression tests were executed on a Zwick Z050 type universal material testing machine at 20 mm/min crosshead speed, between two rigid, flat, parallel plates. Tested specimens were compressed until fractures of the pipe walls, which happened at high crosshead displacements and low forces compared to the 50 kN capacity of the machine and therefore no compliance correction was applied to the test data.

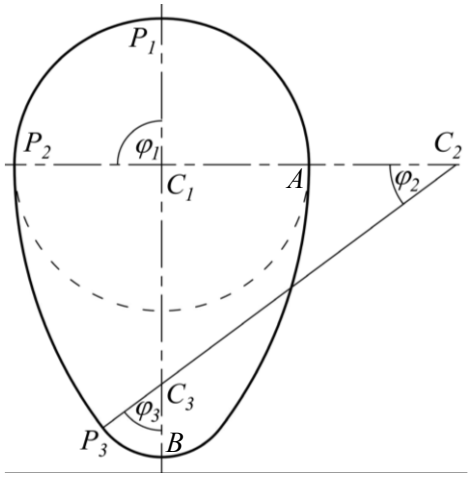

Figure 1. Cross sectional geometry of the tested and modelled egg shape profile pipes

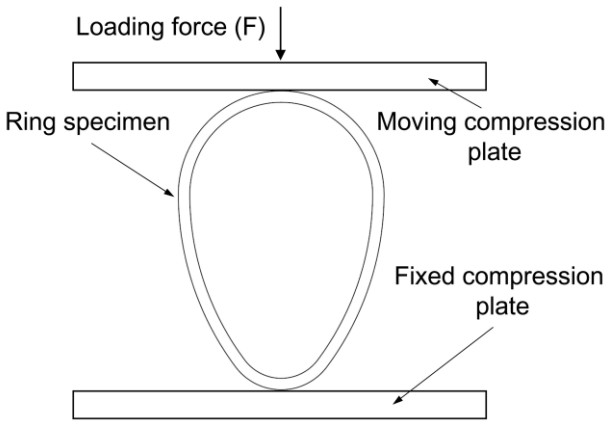

Figure 2. Ring compression test alignment with egg shape profile ring specimen

Nominal geometric properties of the tested rings were the following (see Figure 1.): characteristic mean radius: $R_m = \left|\overline{C_1 P_1}\right| = 80$ mm, nominal wall thickness: t=2.4 mm, length: l=20; 40; 80; 160 mm, cross- sectional height: $h=3R_m$=240 mm, cross- sectional width: $b=2R_m$=160 mm. Three specimens were tested from each different lengths except for the longest type, where only one specimen was tested (altogether 10 pieces). Load-displacement graphs were evaluated for the specimens tested.

Matrix material of the examined composite pipe was AOC Altek H557-AEF-30 type orthophthalic acid based unsaturated polyester formulated for filament wound tanks and pipes. Applied reinforcing material was Johns Manville Star Rov PR 300 2400 907 direct E-glass roving with a linear density of 2400 tex. The roving was manufactured with silane sizing, which provides excellent adhesion to unsaturated polyester.

The tested pipes were manufactured by filament winding technology at Hodács Composites Ltd. (Hungary) with a winding angle θ=83.5±1.3° to the longitudinal axis of the pipe. The composite material was cured at room temperature for 24 hours and postcured at 60°C for 6 hours. The fibre weight fraction of the tested composite pipes was examined with the burning method according to ISO 3451-1 and found to be v_m =71.4±2m%. As the density of reinforcing fibres is almost two times higher than that of the matrix material, the fibre content was calculated into volume fraction to give more relevant information on the material composition. The density of the composite material was examined according to ISO 1183-1 with the immersion method and found to be ρ_c=1.924±0.03 g/cm^3. The glass fibre volume fraction calculated with the measured density of the composite material was v_f=53.9±2.2V%.

3. FE modelling of the ring compression tests

In this section the finite element model applied for simulating the ring compression tests is discussed in details. This setup has been chosen as a verification of the FE model developed, because experimental results were available for comparison. Initial attempts to find the most accurate modelling strategy is not presented, but as a result of assessments on several different 2D and 3D models including shell and body types, 3D body modelling has been chosen after comparison with test results.

3.1. Material definition

During the modelling phase the notable anisotropy of the filament wound pipe material was taken into account, although it was treated as a quasi-homogenous material. This

simplification is acceptable, as the scope of the analysis was to assess the global behaviour of the tested composite rings. Material characteristics were set to be linearly elastic as glass/polyester composites are usually brittle, and fail without notable irreversible deformations. Parameters of nonlinear material models would be too difficult to obtain and the emphasis of the study was on the elastic response, not on damage modelling. Due to large displacements, geometrically nonlinear analysis was performed. Material properties of the constituents of the composite material were defined based on technical datasheets and literature data of the constituents given in Table 1.

Table 1. Elastic properties of the composite constituents, where *E*- elastic modulus, ν- Poisson's ratio, *G*- shear modulus

Property	*E*	ν	*G*
Unit	[GPa]	[-]	[GPa]
Glass fiber (*f* index)	72	0.22	33
Unsaturated polyester (*m* index)	3	0.33	1

Using the elastic properties of the constituents and the rules of mixtures [21] the engineering constants of a transversely isotropic unidirectional (UD) layer was calculated. This layer, with appropriate fiber volume fraction can be treated as a basic element of a filament wound pipe wall. The on-axis (parallel to fibre direction) elastic modulus of the UD ply was calculated with Equation (1):

$$E_1 = \nu_f \cdot E_f + \left(1 - \nu_f\right) \cdot E_m \tag{1}$$

where E_1 is the on-axis elastic modulus of the UD ply, E_f is the elastic modulus of the fibre, E_m is the elastic modulus of the matrix material, and v_f is the fibre volume fraction. The transverse direction elastic modulus E_2 of the UD ply was calculated using the modified rule of mixture [21] (Equation (2)), because it is reported to be more accurate and still simple.

$$E_2 = \left(\frac{\sqrt{\nu_f}}{E_b} + \frac{1 - \sqrt{\nu_f}}{E_m} \right)^{-1} \quad \text{where} \quad E_b = \sqrt{\nu_f} \cdot E_f + \left(1 - \sqrt{\nu_f}\right) \cdot E_m \tag{2}$$

The Poisson's ratio ν and the shear modulus of elasticity G_{12} can be calculated with the rule of mixture, and the modified rule of mixture respectively. Table 2. shows the engineering constants of the defined transversely isotropic UD composite ply.

Table 2. Elastic properties of the defined UD composite ply where E_1 and E_2 are elastic moduli of the ply in on-axis and transverse direction respectively, ν_{12} is the Poisson's ratio and G_{12} is the in-plane shear modulus of the ply (v_f=54 V%).

Property	E_1	E_2	ν_{12}	G_{12}
Unit	[GPa]	[GPa]	[-]	[GPa]
Value	40.26	9.8	0.27	3.39

The compliance and the stiffness matrices are needed for further calculations. Definitions are given for transversely isotropic materials in Equations (3), (4).

$$\left[S^0\right]=\begin{bmatrix} \frac{1}{E_1} & -\frac{\nu_{12}}{E_1} & -\frac{\nu_{12}}{E_1} & 0 & 0 & 0 \\ -\frac{\nu_{12}}{E_1} & \frac{1}{E_2} & -\frac{\nu_{23}}{E_2} & 0 & 0 & 0 \\ -\frac{\nu_{12}}{E_1} & -\frac{\nu_{23}}{E_2} & \frac{1}{E_2} & 0 & 0 & 0 \\ 0 & 0 & 0 & \frac{2\cdot(1+\nu_{23})}{E_2} & 0 & 0 \\ 0 & 0 & 0 & 0 & \frac{1}{G_{12}} & 0 \\ 0 & 0 & 0 & 0 & 0 & \frac{1}{G_{12}} \end{bmatrix} \tag{3}$$

$$[C^0]=[S^0]^{-1} \tag{4}$$

where $[S^0]$, $[C^0]$ refers to the compliance and the stiffness matrices respectively and uppercase 0 refers to the direction of the local coordinate system with respect to the fibre direction in degrees. As in case of a transversely isotropic composite layer, index 1 refers to the fibre direction and indexes 2 and 3 can be commuted, there is only one material property ν_{23} left in the compliance matrix which is not listed in table 2. Since ν_{23} is associated with the out of plane stresses, that are often negligible in case of thin composite plates, it has no significant effect during the modelling. The significance of ν_{23} was analyzed in the sensible range and confirmed not to effect the characteristics of a pipe wall model under ring compression notably. Finally ν_{23} was set to 0.3 as it is close to the value of the matrix material. The next step towards the definition of the pipe wall material was the generation of a homogenised layer of the biaxial structure of the filament wound composite. The structure of the pipe-wall was similar to that of a fabric with 2x6.5° angle between the yarns. Such a structure results in orthotropy with respect to the bisector of the yarn angle. In case of the filament wound

structure of the tested pipes the equivalent of the usually narrow and perpendicularly aligned yarns in weaves were 32 mm wide tapes of six 2400 tex E-glass filaments wound under low angles to cover half of the area of the tool in one run (one direction). In order to cover the tool completely, two forth and back runs has to be performed by the fibre carriage. The specific setup of the filament winding process resulted in a quasi-symmetric, balanced layer of four ±6.5° pseudo-fabric plies. Stiffness matrix of this homogenised layer can be calculated by averaging the stiffness matrices of two counter-aligned UD plies, as shown by Equation (5).

$$\left[C^{\pm 6.5}\right] = \frac{1}{2}\left(\left[C^{+6.5}\right] + \left[C^{-6.5}\right]\right) \tag{5}$$

where uppercase numbers shows the alignment of the UD plies with respect to the circumferential direction of the pipe in degrees. Rotation of the stiffness matrices can be done by simple mathematical formulae, using the trigonometric functions of the rotational angles. After inverting the stiffness matrix of the homogenised layer $[C^{\pm 6.5}]$ the engineering constants can be calculated from $[S^{\pm 6.5}]$, using the definition of [S] for orthotropic properties according to Equation (6).

$$[S] = \begin{bmatrix} \frac{1}{E_1} & -\frac{\nu_{21}}{E_2} & -\frac{\nu_{31}}{E_3} & 0 & 0 & 0 \\ -\frac{\nu_{12}}{E_1} & \frac{1}{E_2} & -\frac{\nu_{32}}{E_3} & 0 & 0 & 0 \\ -\frac{\nu_{13}}{E_1} & -\frac{\nu_{23}}{E_2} & \frac{1}{E_3} & 0 & 0 & 0 \\ 0 & 0 & 0 & \frac{1}{G_{23}} & 0 & 0 \\ 0 & 0 & 0 & 0 & \frac{1}{G_{13}} & 0 \\ 0 & 0 & 0 & 0 & 0 & \frac{1}{G_{12}} \end{bmatrix} \tag{6}$$

Table 3. shows the engineering constants of the homogenised layer of the modelled filament wound pipe wall.

Table 3. Engineering constants of the orthotropic, filament wound homogenised composite layer representing the wall of the modelled pipes for v_f=54V%

Property	E_1	E_2	E_3	ν_{12}	ν_{13}	ν_{23}	G_{12}	G_{13}	G_{23}
Unit	[GPa]	[GPa]	[GPa]	[-]	[-]	[-]	[GPa]	[GPa]	[GPa]
Value	39.22	9.73	9.81	0.31	0.26	0.30	3.80	3.39	3.76

The presented engineering constants can directly be put into Abaqus with regards to the default orientations. Material orientations of the pipe wall were defined by dividing the modelled rings into partitions, in which the radii of the pipe wall were constants, hence the material directions could be defined in cylindrical coordinate systems.

3.2. Geometry definition

Geometry of the modelled rings was defined in the 3D modelling interface of Abaqus, by creating connected cylindrical partitions of the meshed part. Symmetry of the ring specimen with respect to both vertical planes provided the possibility of modelling and meshing only one quarter of each ring specimen, as shown in green in Figure 3.

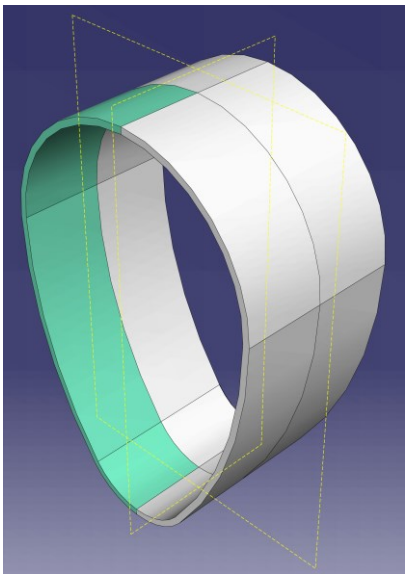

Figure 3. Geometry and symmetry planes of a modelled ring (l=80 mm)

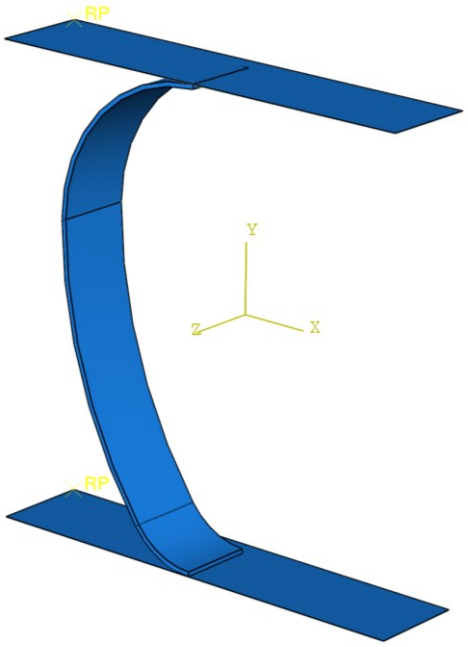

Figure 4. FE model assembly of the ring compression test setup

The thick steel compression plates were modelled as analytical rigid bodies, due to the relatively low contact forces and their significantly higher stiffness compared to the fibreglass reinforced composite rings. Figure 4. shows the assembled geometry of the ring compression test alignment.

3.3. Meshing

According to a sensitivity study, certain layers of linear and quadratic brick elements were applied across the pipe wall. It was found that quadratic brick elements are more suitable, because they give more accurate results even if only two rows of elements are used along the pipe wall. Figure 5. shows the convergence of an overall normalized output (reaction force integrated on the upper compression plate at a certain vertical displacement).

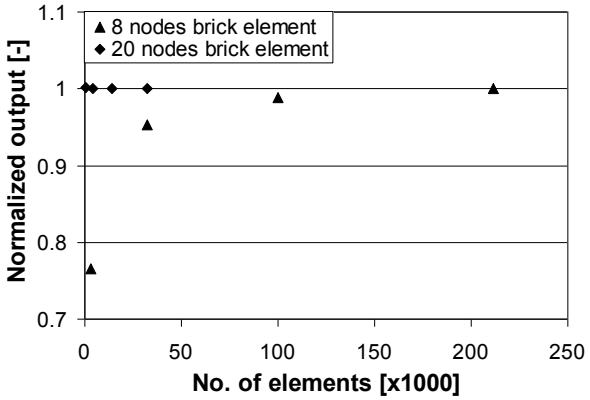

Figure 5. Results of sensitivity study on element type and size

Assuming the limited number of models to be constructed, 2 layers of equal volume 20 node quadratic brick elements were applied through the pipe thickness.

3.4. Boundary conditions, constraints, loads

Contact properties were introduced between contact surfaces of the elastic body (composite pipe) and the analytical rigid bodies (compression plates) according to Figure 4. The contact properties in the normal direction was assumed to be hard and in the tangential direction frictionless behaviour was set, as no notable sliding was expected. Two planes of symmetry were defined in the vertical directions, which blocked all degrees of freedom of the elastic body except for vertical displacement. This was blocked by the analytical rigid bodies, from which the lower was fixed, and certain vertical displacement was set for the upper. As the Abaqus standard solver applies load or displacement in increments, displacement controlled ring compression tests could be simulated using the time history outputs.

4. Verification results and discussion

The reaction forces integrated on the modelled upper compression plate were compared to the experimentally obtained compression forces from the ring compression tests executed. Figure 6. shows the experimental and modelled compression curves for the four specimen types.

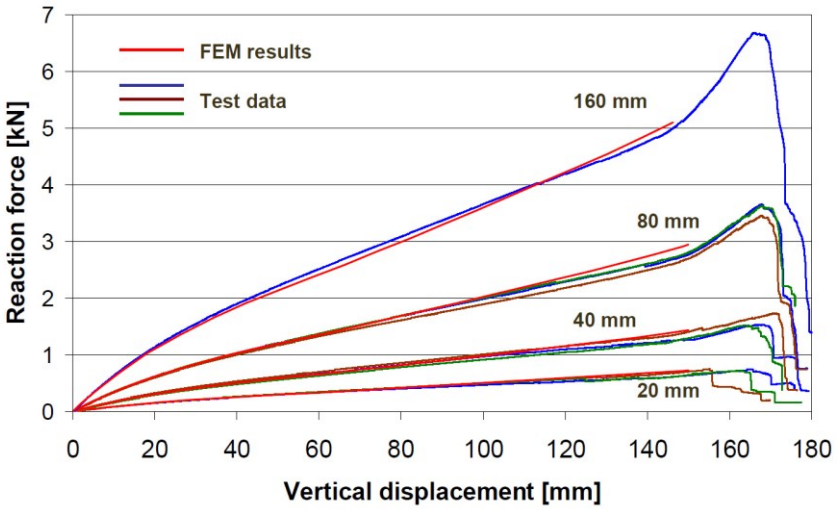

Figure 6. Comparison of experimental and modelled compression force-displacement curves for different specimen lengths

Overall good agreement between experimental and modelling results is obvious from Figure 6., especially in the initial (0-100 mm) displacement range, where no damage were observed in the specimens during the tests. First failures appeared in the 100-150 mm displacement range, where therefore all the test curves run below the corresponding FEM curves, because no damage criterion were involved in the model. The changes in slopes around 150 mm vertical displacement on the experimental curves correspond to the event, when the highest radius side sections of the specimens come into contact with the compression plates. As it is far beyond the application limits of the composite pipes, this displacement regime was not modelled. Despite highly visible global agreement between the experimental results and the model outputs, the accuracy of the model was analyzed by checking the relative difference between the average of the experimental and the single modelled reaction forces at 10 equally spread displacement values in the 0-100 mm range for each specimen length. Equation 7. defines the *D* deviation values.

$$D = \frac{\sum_{i=1}^{10} \frac{\left| EXP_{avi} - FEM_i \right|}{EXP_{avi}}}{10} \tag{7}$$

Where *D* is the average normalised absolute deviation for a specified specimen length, $EXP_{av\,i}$ is the average of the experimental reaction forces and FEM_i is the modelled reaction force at a specified displacement. Table 4. shows the *D* values for the different specimen lengths. The

low deviations (under 3%) prove that the developed FE model is capable of the global stiffness modelling of non circular profile composite pipes.

Table 4. Average normalised absolute deflections of reaction forces under ring compression for different specimen lengths

Specimen length [mm]	20	40	80	160
D [%]	1.11	1.12	1.27	2.99

5. New design methodology

This section gives details on the subsequent steps of the development of the new design methodology for egg shape profile composite liner pipes.

5.1. Pipe-in-pipe FE model and parametric study

After the verification of the FE model under ring compression alignment, a more complex model was developed, which was capable of simulating the operational loads and displacements of a flexible polymer composite liner in a rigid encapsulating old pipe with a certain gap between them. In case of this so called pipe-in-pipe system, it is common to assume that the static condition of the old pipe is satisfactory, and the liner is inserted in order to restore the water tightness of the system. In such an alignment, the old pipe can be modelled as an analytical rigid body, and the only active load on the linearly elastic composite liner is the hydrostatic outer pressure of the groundwater table. The usually negligible gravity forces, acting on the liner pipe, were also taken into account. The hydrostatic pressures applied in this study were in the range of 0-0.4 MPa which is higher than the usual actual loads, as the maximum value corresponds to around 40 m of groundwater table. However there are certain lining technologies, where cement mortar is injected in the gap between the old and the liner pipe under low pressure, possibly in the mentioned range. The material property and orientation definition was done in the same way as earlier for the ring compression test model. The contact definition and properties were also identical to the previous study. The pipe-in-pipe model also took only one quarter of the elastic liner pipe into account due to symmetries along the two perpendicular vertical planes as earlier. Figure 7. shows the geometry of the assembled model. The elastic body of the liner pipe was fixed at one of the upper nodes, because as a result of the hydrostatic pressure (normally producing higher vertical forces than the weight of the liner) the liner pipe is “floating” up against the rigid old pipe. As the scope of this study is to develop a design tool for engineers which can be applied without using one of the expensive finite element modelling software packages, the

stress and displacement distributions on the elastic body were not analysed in details. The focus was on the global impact of material and geometrical parameters on the stiffness of the liner pipe.

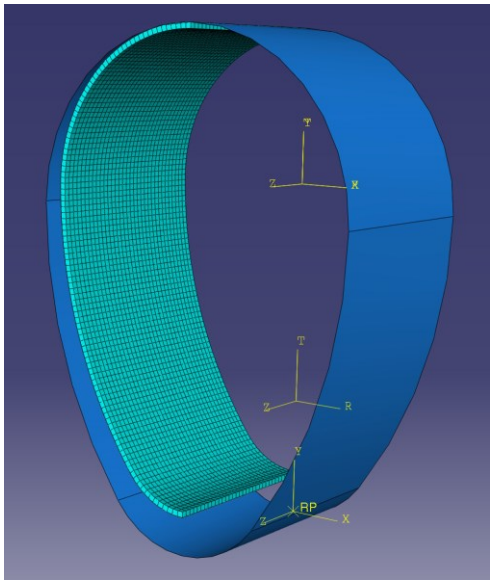

Figure 7. Assembly of the pipe-in-pipe model with mesh on the elastic body

The most important parameters were considered to be the following three: 1. the **fibre volume fraction**- v_f, 2. the **winding angle**- θ (measured with respect to the circumferential direction) of the filament wound fibre reinforced composite liner pipes and 3. the **wall thickness**- t of the liner pipe. The material related parameters were taken into account in the previously detailed procedure for material definition and various wall thicknesses were simply incorporated in the FE model geometry. The stiffness of the pipe-in-pipe model can be defined using the horizontal displacement (intrusion) of point A on the elastic pipe wall (see Figure 1.) in function of the applied outer hydrostatic pressure. If the section geometry - including the gap between the rigid and the elastic pipes- and the elastic properties of the constituents of the composite pipe are constant, the stiffness of the liner pipe is fully determined by the three input parameters mentioned above. Figure 8. shows the horizontal displacements u_x of point A on the liner pipe in function of the applied outer pressure in a typical model case.

a) b)

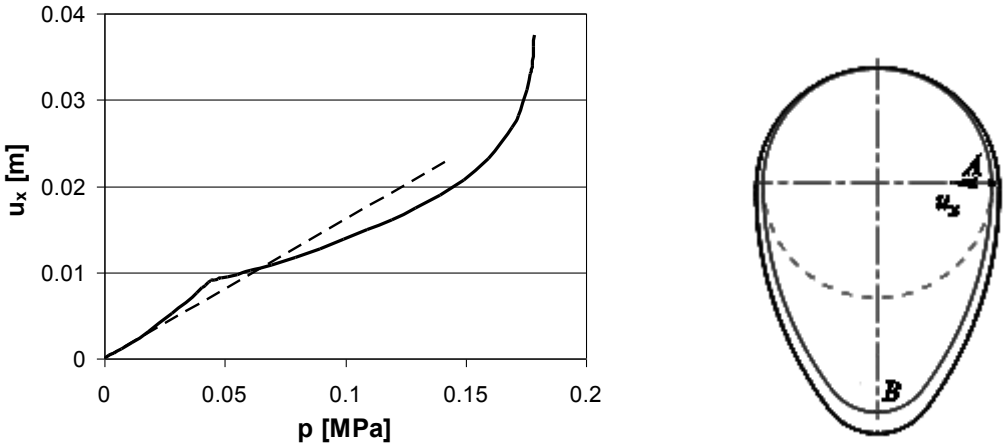

Figure 8. a) Typical outer pressure- horizontal displacement curve of a pipe-in-pipe model with a dashed line showing the initial slope b) Schematic of the displacement definition

An abrupt change of slope on the curve corresponds to the condition when the lower point (*B*) of the liner pipe collides with the rigid old pipe-wall. The final infinitely high slope section of the curve is due to loss of stability which corresponds to the buckling of the section. The stiffness of the pipe section *M* was defined as the initial slope of the curve presented on Figure 8a: $M=\Delta p/\Delta u_x$ where p is the outer pressure and u_x is the horizontal displacement of point *A* on the pipe wall. Table 5. shows the values of the three parameters which were used during a modelling study to establish the stiffness response of the liner pipes with different material and geometrical parameters.

Table 5. Parameter values for the modelling study

v_f [V%]	40	50	60
θ [°]	20	15	10
t [mm]	2.8	3.0	3.2

During the parametric study, 15 combinations of the three parameters were generated in Statistica software, assuming constant 5 mm gap between the liner and the old pipe and p=0.2 MPa outer hydrostatic pressure. All 15 models were run and the *M* stiffness values were evaluated and a 10 parameter function was fitted to them using Statistica. Table 6. shows the parameter combinations, the M_{model} values coming from the models and the $M_{function}$ values of the fitted function at the specified parameter combinations. The normalised deviation values were also calculated to assess the accuracy of the fitted function.

Table 6. Details of the parametric study

No. of par. comb.	v_f [V%]	θ [°]	t [mm]	M_{model} [MPa/m]	$M_{function}$ [MPa/m]	Deviation [%]
1	37.13	15.000	3.000	6.76	6.75	0.215
2	40.00	10.000	2.800	6.21	6.20	0.080
3	40.00	10.000	3.200	9.19	9.24	-0.449
4	40.00	20.000	2.800	5.40	5.41	-0.335
5	40.00	20.000	3.200	8.07	8.03	0.464
6	50.00	15.000	3.000	8.86	8.85	0.147
7	50.00	8.565	3.000	9.52	9.48	0.404
8	50.00	21.435	3.000	7.85	7.90	-0.613
9	50.00	15.000	2.743	6.81	6.81	0.034
10	50.00	15.000	3.257	11.18	11.19	-0.108
11	60.00	10.000	2.800	9.02	9.06	-0.371
12	60.00	10.000	3.200	13.26	13.24	0.166
13	60.00	20.000	2.800	7.85	7.80	0.578
14	60.00	20.000	3.200	11.57	11.57	-0.008
15	62.87	15.000	3.000	10.84	10.86	-0.224

The fitted form of the 10 parameter function is given in Equation (8).

$$M = 11.5\text{-}0.212 \cdot \mathrm{v}_f - 0.000253 \cdot \mathrm{v}_f^2 + 0.415 \cdot \theta - 0.00379 \cdot \theta^2 - 10.9 \cdot t + 2.29 \cdot t^2 - 0.00231 \cdot \mathrm{v}_f \cdot \theta + 0.144 \cdot \mathrm{v}_f \cdot t - 0.103 \cdot \theta \cdot t \quad (8)$$

The accuracy of the fitted function was checked at other 14 parameter combinations within the original range of the parameters and even beyond them in the range of higher stiffness values. The average normalised deviation in the new series of parameter combinations were 0.388% and the highest deviation was 1.93%. According to the low deviation values it can be stated that the fitted function is capable of estimating the stiffness of the liner pipes in the studied parameter range.

5.2. Design chart

The next step of the development of the design method was choosing 8 models with different stiffness values (M=5.4 MPa/m - 17.2 MPa/m) and running their FE models without the constraining rigid body (old pipe) up to p=0.4 MPa outer hydraulic pressures. Figure 9. shows the displacement of point A plotted with positive sign, together with the vertical displacement of point B with negative sign both in function of the outer pressure for each chosen stiffness value.

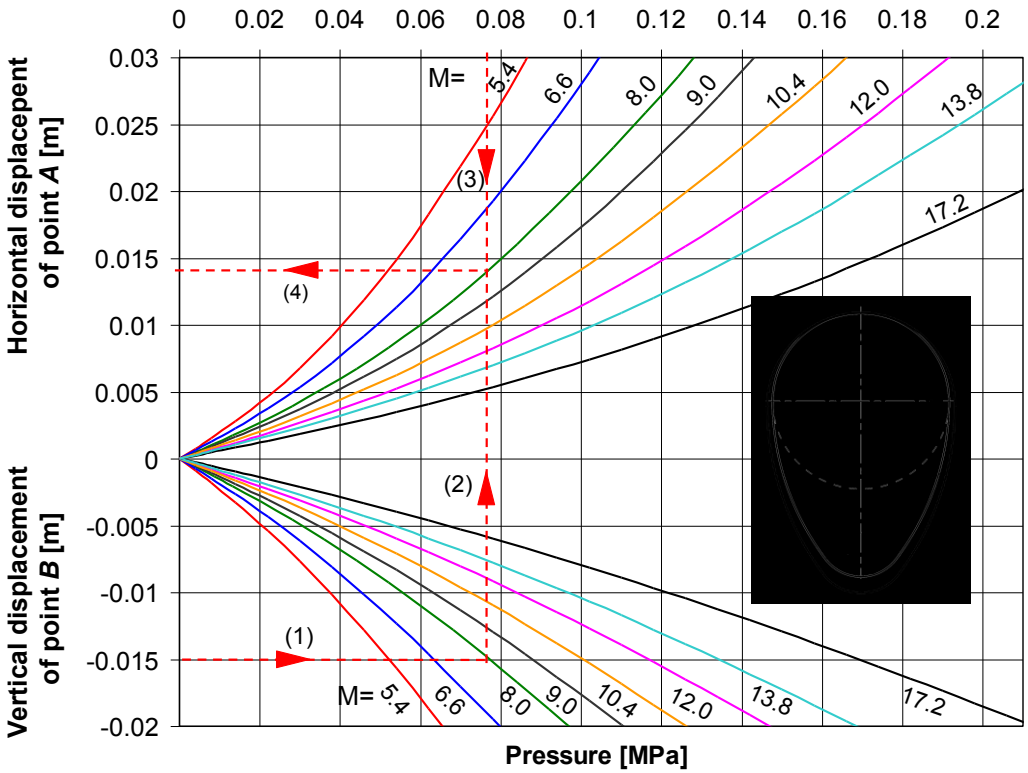

Figure 9. Pressure-displacement curves for liner pipes with various stiffness values (The numbers on the curves indicate the *M* stiffness in [MPa/m], dashed red lines and arrows show an example of use detailed in the text.)

Please note that Figure 9. only shows the range of displacements, which makes engineering sense. For example the vertical displacements of the lower point of the section ranging up to 20 mm means that a maximum gap of 10 mm can be present between the liner and the old pipe, as strong nonlinearity caused by collision between them cannot be handled in this design tool.

Figure 9. for example can be used to determine the pressure, at which the collision between the old and the liner pipe is predicted to happen. Let's assume that the material and geometric parameters are known for a given pipe design, so the *M* stiffness can be calculated with Equation (8). If the size of the gap is known, the designer can prevent vertical displacements higher than twice the size of the gap by projecting the limit vertical displacement horizontally to the coloured line corresponding to the stiffness of the given pipe e.g. *M*=8 MPa/m (1) and then reading the pressure at which the limit displacement is reached (2). The horizontal deformation of the pipe section can be checked at the same condition using the existing vertical line in the positive displacement regime of the chart by finding the intersection with the positive curve of the same stiffness (3), and reading the corresponding displacement from the vertical axis (4). The horizontal displacements can be used to estimate

the change in flow capacity in terms of outer pressure as the section becomes narrower. Calculations can be done the other way round, starting with a given pressure and a limit deformation, and finding the suitable material parameters and wall thickness through the required stiffness of the pipe section.

The developed design procedure is valid for 160/240 mm nominal size egg shape profile pipes (detailed earlier), 0-10 mm gap sizes and 0-0.2 MPa outer pressures. Other geometries and loading conditions need modified FE models and new parametric studies to be performed but the procedure remains the same.

6. Conclusions

- A finite element model was developed to model the ring compression tests of filament wound non-circular profile composite pipes. The model was verified against experimental data, and found to be suitable to analyse the elastic response of non-circular composite pipes.
- A pipe-in-pipe type finite element model was also developed to simulate the operating conditions of the underground composite wastewater pipe linings subject to the outer pressure of the groundwater table.
- A parametric study was performed, and a 10 parameter function was fitted to the model data in order to enable the determination of the defined stiffness of any specific pipe design in terms of the fibre volume fraction, the winding angle and the wall thickness within the boundaries of the study.
- A unique design tool was developed in the final form of a chart representing the deformations of given cross section liner pipes of a wide range of stiffness in function of the applied outer pressure. Once established for a given material and cross section, this cost-effective tool enables design engineers to perform several different quick checks and predictions determining the elastic behaviour of the designed pipe without running finite element models.

Acknowledgement

This work is connected to the scientific program of the "Development of quality-oriented and harmonized R+D+I strategy and functional model at BME" project. This project

is supported by the New Széchenyi Plan (Project ID: TÁMOP-4.2.1/B-09/1/KMR-2010-0002). The authors thank Hodacs Composites Ltd. for manufacturing the test-pipes.

7. References

[1] Lukács. J. Dimensions of Lifetime Management. Material Science Forum 2005;473-474: 361-368.

[2] Downey D. Trenchless technology: a modern solution for clean-flowing cities. Proceedings of the Institution of Civil Engineers – Civil Engineering 2006;159(5):26–30.

[3] Pennington RA, Gersley KA, Gagliostro A, Eagan DT, Zach AL, George JT. Saving a city's sewers. Civil Engineering- ASCE 2008 December.

[4] Basu NB, Boral S, Mndal SK, Dey A. Rehabilitation of Kolkata's first Victorian-age brick sewer. Proceedings of the Institution of Civil Engineers- Municipal Engineer In press. http://dx.doi.org/10.1680/muen.12.00051

[5] Basu NB, Dey A Ghosh D. Kolkata's brick sewer renewal: history, challenges and benefits. Proceedings of the Institution of Civil Engineers – Civil Engineering 2013;166(2):74–81.

[6] Basu NB, Dey A. New life for Kolkata's sewers. Civil Engineering, ASCE 2012;82(7/8):68–75.

[7] Stein D. Rehabilitation and Maintenance of Drains and Sewers. Ernst & Sohn, Berlin, 2001.

[8] C. Madryas C, Wysocki L. Renovation of brick interceptor sewers. Tunnelling and Underground Space Technology 2008;23:718–726.

[9] Boot JC, Welch A. Creep buckling of thin-walled polymeric pipe linings subject to external groundwater pressure. Thin-Walled Structures 1996;24:191-210.

[10] Boot JC. Elastic buckling of cylindrical pipe linings with small imperfections subject to external pressure. Tunelling and Underground Space Technologies 1997;14(1):3-15.

[11] Zhao WZ, Nassar R, Hall D. Design and reliability of pipeline rehabilitation liners. Tunnelling and Underground Space Technology 2005;20:203-212.

[12] Thépot O. Structural design of oval-shaped sewer linings. Thin-Walled Structures 2001;39:499-518.

[13] Thépot O. A new design method for non-circular sewer linings. Trenchless Technology Research 2000;15:25-41.

[14] Timoshenko SP, Gere JM. Theory of elastic stability. McGraw-Hill Companies, 1961.

[15] Wahab MA, Alam MS, Pang SS, Peck JA, Jones RA. Stress analysis of non-conventional composite pipes. Composite Structures 2007;79:125-132.

[16] Guedes RM. Stress-strain analysis of a cylindrical pipe subjected to a transverse load and large deflections. Composite Structures 2009;88:188-194.

[17] Ikram KI, Abdennour CS. Shape Factors for Irregular Glass Reinforced Plastic Pipes – An Analytical and Numerical Approach. Key Engineering Materials 2011;471-472:279-284.

[18] Falter B, Muller-Rochholz J, Eilers J, Gutermann M. Buckling experiments on polyethylene liners with egg-shaped cross-sections. Geosynthetics International 2008;15:152-164.

[19] ATV-M 127-2 Design code: Static Calculation for the Rehabilitation of Drains and Sewers Using Lining and Assembly Procedures. DWA – Deutsche Vereinigung fur Wasserwirtschaft, Abwasser und Abfall e. V. 2000.

[20] Water Research Centre. Sewerage rehabilitation manual. Vol. II. Marlow, UK, 2001.

[21] Kollár LP, Springer GS. Mechanics of composite structures. Cambridge University Press, USA. 2003.